RSC Advances

PAPER

Cite this: *RSC Adv.*, 2018, **8**, 4963

Facile preparation of porous organic copolymer based on triptycene and crown ether for efficient organic dye adsorption†

Ting Xu,[a] Yan He,*[b] Ying Qin,[a] Chengxi Zhao,[a] Changjun Peng,*[a] Jun Hu[a] and Honglai Liu[a]

There has been great interest in the use of porous polymers to remove organic dyes because of their adjustable surface area and task-specific functionality. We chose a triptycene-based porous polymer to ensure high porosity, and introduced crown ether into the sketch of the copolymer to significantly enhance the affinity for the organic dye molecules. Novel porous organic copolymers of triptycene and crown-ether-15 (POP-TCE-15) were obtained by a simple Friedel–Crafts reaction, and were highly effective in removing organic dyes from aqueous solution. POP-TCE-15 exhibited the best performance, with a maximum adsorption capacity of methylene blue, rhodamine B, and methyl orange of 787.4 mg g^{-1}, 421.9 mg g^{-1}, and 64.8 mg g^{-1}, respectively, which is better than most reported adsorbents. Their adsorption rates and adsorption isotherms were well fitted with pseudo-second-order kinetic models and the Langmuir model. More importantly, POP-TCE-15 can be effectively regenerated and recycled at least 5 times without any loss of adsorption capacity. With a hierarchical porous structure, high surface area, high hydrophobicity, and excellent adsorption capacity for dyes, the POP-TCE polymers could be ideal adsorbents for water purification and treatment.

Received 16th November 2017
Accepted 15th January 2018

DOI: 10.1039/c7ra12495c

rsc.li/rsc-advances

Introduction

Many industries such as the textile, pulp and paper, dyestuff, and plastic industries use dyes to color their products.[1] Most of these dyes are toxic and even carcinogenic and present a severe hazard to aquatic living organisms.[2] Therefore, it is necessary to eliminate them before discharging. Generally, adsorption using adsorbent has been recognized as the most practical method for this purpose.[3–5] Traditional porous materials such as activated carbon,[6] zeolites,[3,7] and mesoporous silica[8] have the disadvantage of low adsorption capacities. To facilitate the efficiency of removing organic dyes, many advanced adsorbents such as carbon nanotubes,[9] porous BN nanosheets,[10] and porous graphene[11] have been developed. However, because multi-step synthesis is necessary to produce these functionalized porous polymers, further applications may potentially be limited. Because of the current limitations, exploring novel porous adsorbents for efficient adsorption and removal of dyes is still of great significance and challenge.

During the past decade, porous organic polymers (POPs) have attracted increasing attention because of their high surface areas, good porosities, high stability, and structural diversity. Many types of functional POPs have been reported to have potential in catalysis,[12–14] adsorption,[15–17] gas storage and separation,[18–20] conductivity and optoelectronics[21,22] and other applications. It is believed that the atoms with lone pair electrons, such as O and N in the functionalized groups, may significantly enhance cationic dye removal. In fact, a recent study on an amino-MIL-101(Al)[23] has demonstrated that an electrostatic interaction occurs between the amino group and cationic dye methylene blue (MEB). To the best of our knowledge, the application of porous organic copolymer with a lone pair of electrons in the O atom in the crown ether for dye removal has never been reported.

In this study, we report a novel hydrophobic porous organic copolymer with triptycene and crown ether-15 (POP-TCE-15) as the adsorbent for the removal of dyes such as MEB, RhB (rhodamine B), and MO (methyl orange). POP-TCE-15 displayed extraordinary adsorption capacity for the cationic dye MEB. The adsorption kinetics, isotherms, and regeneration of the adsorbent for the removal of MEB, RhB, and MO were studied in detail. Additionally, the mechanism of adsorption of the dyes on POP-TCE-15 was tentatively illustrated by theoretical quantum calculation. Hence, the fast adsorption kinetics, large adsorption capacity, excellent chemical stability, and good reusability make POP-TCE-15 an adsorbent with great potential for the removal of dyes from water.

[a]School of Chemistry and Molecular Engineering, East China University of Science and Technology, Shanghai 200237, China. E-mail: cjpeng@ecust.edu.cn
[b]Jiangxi Province Key Laboratory of Polymer Micro/Nano Manufacturing and Devices, School of Chemistry, Biology and Materials Science, East China University of Technology, Nanchang, 330013, People's Republic of China. E-mail: yanhe@ecit.cn

† Electronic supplementary information (ESI) available. See DOI: 10.1039/c7ra12495c

Experimental

Materials

All purchased chemicals were at least reagent grade and were used without further purification. Triptycene (98.0%), anhydrous ferric chloride ($FeCl_3$, ≥98.0%), 1,2-dichloroethane (DCE, 99.8%), and formaldehyde dimethyl acetal (FDA, ≥98.0%) were purchased from Sigma-Aldrich. Crown-ether-15 (98.0%) and all other solvents were purchased from TCI America. Deionized water was used to prepare all aqueous solutions.

Synthesis of porous organic copolymer POP-TCE-15

As shown in Scheme 1, triptycene (0.636 g, 2.5 mmol) and crown-ether-15 (0.224 g, 0.8 mmol) were dissolved in anhydrous 1,2-dichloroethane (20 mL). To this solution, formaldehyde dimethyl acetal (FDA, 0.67 mL) and anhydrous $FeCl_3$ (1.22 g, 7.5 mmol) were added under a nitrogen environment. The resulting reaction was carried out at 45 °C for 5 hours and then raised to 80 °C for 19 h with constant stirring. After cooling to room temperature, the crude product was collected by filtration and repeatedly washed with methanol until the filtrate nearly colorless. The product was further purified by Soxhlet extraction in methanol for 24 h. Finally, the product was dried in vacuum at 80 °C for 24 h to provide POP-TCE-15 as a brown powder with a yield in excess of 100%, which might be due to the trapping of iron residues within the networks or the adsorption of some guest molecules such as organic solvents, water, and CO_2 within the networks.

Instruments and characterization

The thermal stability was detected using a thermal gravimetric analysis (TGA) unit (NETZSCH STA 499 F3). Approximately 10 mg of the sample was heated from ambient temperature to 900 °C at a heating rate of 10 °C min^{-1} in nitrogen with a flow rate of 20 mL min^{-1}. The morphology of samples was characterized using a Nova NanoS 450 field emission scanning electron microscope (FE-SEM). Transmission electron microscopy (TEM) and high-resolution transmission electron microscopy (HR-TEM) images were recorded using a JEM-2100. The powder samples were treated in ethanol by ultrasound for 20 min then dropped and dried on carbon-coated copper grids. N_2 adsorption–desorption isotherms at 77 K were measured by a volumetric adsorption analyzer (Micromeritics ASAP 3020). Before adsorption measurements, the samples were degassed at 120 °C for 24 h. The specific surface area was calculated using the Brunauer–Emmett–Teller (BET) method and the Langmuir method. The total volume was calculated at $p/p_0 = 0.99$. The micropore volume was derived from the *t*-plot method. Further confirmation and quantification of the hydrophobicity were obtained from contact angle measurements. Tablets of POP-TCE-15 were pressed using a tablet press machine, and a load of 30 kPa was applied to an area of 160 mm^2 using roughly 80 mg of material. Next, 5 μL of deionized water was dropped onto the surface of POP-TCE-15 powder packed on a glass surface, and the contact angle was determined with a JC2000D1 contact angle goniometer. The ultraviolet (UV) spectrum was measured with a Shimadzu UV-2550 spectrophotometer. The scan rate was 240 nm min^{-1}, and the spectral resolution was 2 nm over the spectral region of interest. Solid-state ^{13}C NMR spectra were recorded with a Bruker AV III 400 MHz spectrometer.

Scheme 1 Schematic representation of the synthesis of copolymer POP-TCE-15.

Organic dye adsorption

To examine dye adsorption properties, 2.5 mg of porous organic copolymer POP-TCE-15 was added to 5 mL of different concentrations of MEB, RhB, and MO solution under mechanical shaking at room temperature, and then the adsorbent was filtered with 0.45 μm Millipore cellulose membranes after adsorption. The initial concentration of organic dyes varied from 10 ppm to 1000 ppm. The pH was adjusted by adding 0.01 M HCl or 0.1 M NaOH solution. The residual concentration of dyes at equilibrium and at any time was determined at the maximum wavelength using a UV-Vis spectrophotometer (UV-2550) ($\lambda_{max} = 665$ nm for MEB, $\lambda_{max} = 554$ nm for RhB, $\lambda_{max} = 463$ nm for MO). The adsorption capacity and removal percentage of dyes were calculated using the following equations:

$$q_e = \frac{(C_0 - C_e) \times V}{m} \quad (1)$$

$$E\% = \frac{(C_0 - C_e)}{C_0} \times 100\% \quad (2)$$

where q_e and $E\%$ denote the adsorption capacity (mg g^{-1}) and removal percentage of organic dyes, respectively; C_0 and C_e denote the initial and equilibrium concentrations (mg L^{-1}) of organic dyes in aqueous solution, respectively; V denotes the volume of adsorption solution (mL); and m denotes the weight of the adsorbent (mg).

Desorption experiments and reusability

The adsorption/desorption cycles were conducted as follows: each adsorption experiment consisted of combining 50 mg of POP-TCE-15 with 100 mL of 20 ppm MEB solution for 24 h. After the adsorption experiments, the dye-loaded powder in the flask was collected by filtration, washed with deionized water, and stirred in water/ethanol for 24 h to desorbed the dyes. The regeneration adsorbent was then filtered and separated from the solution, and washed with deionized water. Finally, the regenerated adsorbent was dried at 60 °C under vacuum. The desorption efficiency (%) was calculated as the mass of analyte in dyes desorbed to the elution medium divided by the total

mass of analyte adsorbed on the adsorbent. The above cycle was repeated 5 times.

Quantum calculations

All the molecules were fully optimized using the B3LYP[24,25] method combined with the 6-311G(d,p)[26] basis set for all the atoms involved. During the calculations, no symmetry constraint was performed. Additionally, frequency analysis was calculated using the same theoretical method with the same basis set to ensure that the configurations found were all real minima on the potential energy surface. All the calculations were performed with the Gaussian 09 (ref. 27) software together with the Multiwfn program,[28] version 3.4.1.

Results and discussion

The structure of POP-TCE-15 was characterized by ^{13}C NMR and FTIR. As shown in Fig. 1a, the peaks at 124.2 ppm, 125.7 ppm, and 144.3 ppm are ascribed to the carbon atoms in the aromatic systems. Additionally, the peak at 37.5 ppm indicates the methylene carbon formed by the Friedel–Crafts alkylation reaction. The peak at 54.7 ppm (–OCH_3) resonance indicates secondary reaction channels involving FDA during the polymerization.[29] The presence of –OCH_2– (73.5 ppm) resonance indicates the presence of the crown ether. Furthermore, in the FTIR spectra of POP-TCE-15 (Fig. 1b), the peaks at 1600 cm^{-1}, 1500 cm^{-1}, and 1450 cm^{-1} are attributed to aromatic ring skeletal vibrations. The characteristic bands at 2866 cm^{-1} are assigned to the C–H stretching bands of methylene. The C–O stretching bands of crown ether were observed at 1131 cm^{-1}. In addition, we measured the oxygen content of the copolymer by elemental analysis, which was 8.49%. These ^{13}C NMR, FTIR, and EA results confirmed the successful formation of porous organic copolymer POP-TCE-15.

TGA shows that POP-TCE-15 is stable up to 320 °C under nitrogen (Fig. S1, ESI†). Small mass loss observed below 100 °C is most likely caused by the release of entrapped solvent or small gaseous molecules in the micropores that cannot be removed even in a vacuum. When the temperature reaches 320 °C, a sharp loss of sample mass is observed due to the decomposition of the polymer frameworks. The obtained POP-TCE-15 is insoluble in dilute solutions of NaOH and HCl, as well as common organic solvents, such as dichloromethane, acetone, methanol, THF, and DMF, indicating good chemical stability of the POP-TCE-15 adsorbent polymer.

The morphology, and hydrophobic and crystalline nature of POP-TCE-15 are shown in Fig. 2. The FE-SEM image (Fig. 2a) suggests that POP-TCE-15 consists of aggregated particles without a specific morphology. Moreover, there were many pores in the surface of the POP-TCE-15. The static contact angle (CA) of POP-TCE-15 was measured to characterize the wettability of the polymer surfaces. The water contact angle (WCA) on the copolymer POP-TCE-15 is 115° ± 3.1° (inset in Fig. 2a), exhibiting significant hydrophobicity. The TEM image (Fig. 2b) provides further clear evidence that POP-TCE-15 is composed of amorphous micropores. In addition, without any characteristic peaks in the XRD pattern (Fig. S2, ESI†), the results confirm the amorphous nature of POP-TCE-15. The porosity of POP-TCE-15 was evaluated by the nitrogen adsorption–desorption isotherms at 77 K, and their properties are summarized in Table S1.† Fig. 3a shows the presence of a hysteresis loop in the pressure region of $p/p_0 = 0.2$–0.8 in the N_2 adsorption–desorption curve of the copolymer, which suggests a partial mesoporous character. The hysteresis loop up to a relative pressure above 0.9 suggests the existence of macropores and interparticular voids.[30] Furthermore, the pore size distribution (PSD) curve (Fig. 3b) calculated based on the nonlocal density functional theory (NDFT) further confirms the presence of both micropore (approximately 0.8 nm) and mesopore (approximately 2.5 nm). As summarized in Table S1,† the BET surface area is 848.27 $m^2\ g^{-1}$, which is comparable to the BET surface area of the other porous polymers[3,31] used for dye removal.

Considering the high surface area, good porosity, hydrophobicity, and abundant crown ether groups of POP-TCE-15, the removal of dyes by polymer was studied. The effect of pH

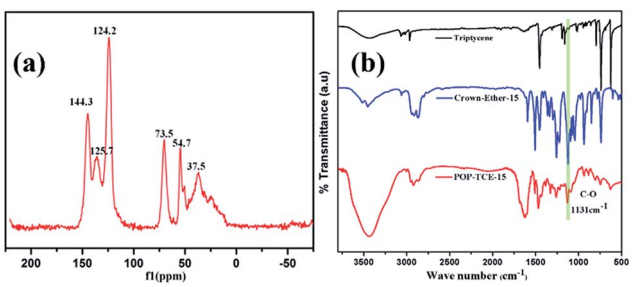

Fig. 1 (a) The ^{13}C NMR of the copolymer POP-TCE-15 and (b) FTIR spectra of triptycene, crown-ether-15, and porous copolymer POP-TCE-15.

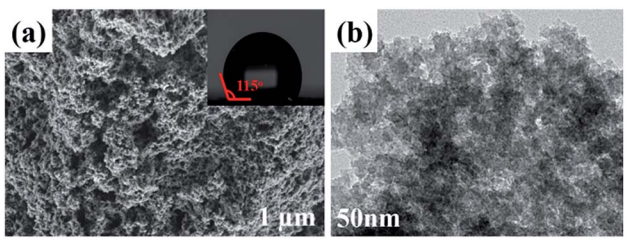

Fig. 2 (a) SEM and (b) HR-TEM images and (inset of (a)) water contact angle of POP-TCE-15.

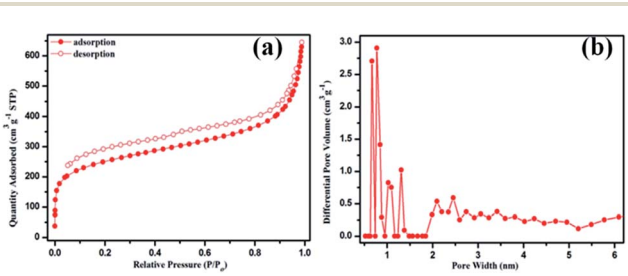

Fig. 3 (a) N_2 adsorption–desorption isotherms and (b) pore size distributions of POP-TCE-15 at 77 K.

from 2 to 9 on MEB, RhB, and MO adsorption is presented in Fig. S3.† There was nearly no change in the percentage removal of MEB and RhB by POP-TCE-15 as the pH increased. However, a lower percentage of MO removal was observed at pH 7–9. With increasing pH values, low adsorption of MO was observed due to the competitive adsorption between MO anions and available OH^- ions of the active sites of the adsorbent. Additionally, the strong electrostatic repulsion prevents the MO ions from approaching the surfaces of the POP-TCE-15, resulting in relatively less adsorption of MO at pH 7–9. Subsequent adsorption experiments were carried out at pH 6.0 unless otherwise stated. The capacity of POP-TCE-15 to adsorb MEB, RhB, and MO was examined at 30 °C (Fig. 4). It can be observed that the adsorption sharply increases within 60 min and slows down thereafter once equilibrium is reached. For cationic dyes MEB and RhB, the equilibrium time was 100 min, which was faster than that of other materials.[32,33] However, for the anionic dye MO, the equilibrium time was 500 min because additional time was required for MO to enter the pores due to the weak relationship between MO and POP-TCE-15.

To analyze the adsorption kinetics of POP-TCE-15, the adsorption data in Fig. 4a were fitted with pseudo-first-order and pseudo-second-order kinetic models (Fig. S4, ESI†). An extremely high correlation coefficient ($R^2 > 0.99$) was obtained for the pseudo-second-order kinetic model (Table S2, ESI†). This suggests that the rate of adsorption of dyes on POP-TCE-15 adsorbent depends on the availability of adsorption sites. Furthermore, the diffusion of dyes also plays an important role in addition to the adsorption itself. The diffusion model proposed by Weber and Morris is commonly used to explain the diffusion mechanism of the adsorption process.[34] Fig. 4b shows that in the multilinear plots of q_t *versus* $t^{1/2}$, there are intercept values of $t^{1/2}$ that are far from zero, which indicates that intraparticle diffusion is not the rate-controlling step of the adsorption process and that the external mass transfer may be significant in the rate-controlling step. The first region describes the external resistance to mass transfer and the second region is attributed to intraparticle diffusion. In the second region, the intraparticle diffusion begins to slow down due to the decrease in dye concentration in the aqueous phase, as well as the decrease of active sites available for adsorption.

Moreover, the adsorption isotherm of POP-TCE-15 is described by the Langmuir and Freundlich models in Fig. 5. The correlation coefficients of $R^2 = 0.995$ and $R^2 = 0.959$ were

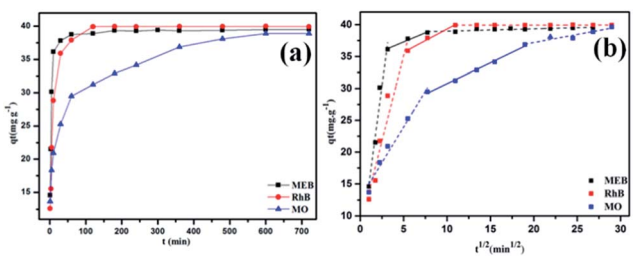

Fig. 4 (a) The effect of time on dye adsorption on POP-TCE-15 and (b) plots of q_t *versus* $t^{1/2}$ of intraparticle diffusion model for the dye adsorption on POP-TCE-15.

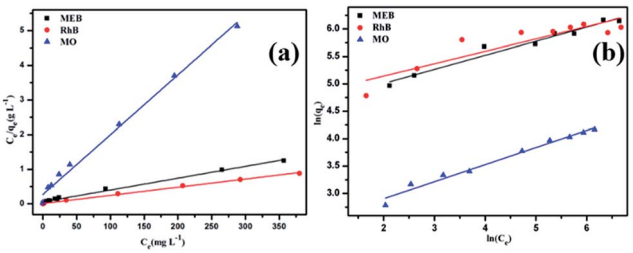

Fig. 5 Two different adsorption isotherms of dyes on POP-TCE-15 based on (a) the Langmuir isotherm model and (b) the Freundlich isotherm model.

obtained for the Langmuir and Freundlich models, respectively, at 30 °C (Table S3, ESI†). This indicates that the experimental data fits better with the Langmuir model, which indicates that the dye is adsorbing on POP-TCE-15 in a monolayer. Furthermore, the maximum adsorption capacity (q_{max}) on POP-TCE-15 evaluated by the Langmuir model is in the sequence of MEB (787.4 mg g^{-1}) > RhB (421.9 mg g^{-1}) ≫ MO (64.8 mg g^{-1}). A comparison with other reported adsorbent polymers is summarized in Table 1. The adsorption capacity for MEB is not as high when compared to covalent organic frameworks (COFs),[39] but the facile preparation process, good recyclability, and low cost of POP-TCE-15 are more favorable for wastewater treatment. Triptycene-based hypercrosslinked polymer sponge (THPS)[38] was obtained by polymerizing triptycene itself. Although THPS has a higher BET surface area, the capacity of POP-TCE-15 to adsorb MEB is still higher due to the effect of electrostatic interaction. Therefore, this novel copolymer POP-TCE-15 adsorbent can be recommended as an efficient alternative for cationic dye removal.

To achieve a deeper understanding regarding the adsorption mechanism of the MEB, RhB, and MO dyes on POP-TCE-15, we employed theoretical quantum calculations to analyze the structural property and electrostatic potential (ESP) of the three dyes and crown-ether-15 compounds.

As shown in Fig. 6, it can be clearly seen that the size of these dyes are in the order of RhB > MO > MEB. If only the size effect

Table 1 Comparison of the maximum equilibrium adsorption capacity of the dyes on different adsorbents at room temperature

Adsorbents	BET surface area (m^2 g^{-1})	q_{max} (mg g^{-1}) of MEB	Ref.
ZIF-67	—	19.6	3
Porous BN nanosheets	1427	313	10
TPP-NH_2	863	204.9	17
Amino-MIL-101(Al)	1980	762.00	23
Fe_3O_4/Mt	147.92	106.38	35
AC	1688	270.27	36
GO	32	243.90	36
CNT	177	188.68	36
PDA microsphere	13.77	90.70	37
THPS	1426	330	38
COF	1484	1691	39
POP-TCE-15	848.27	787.4	This work

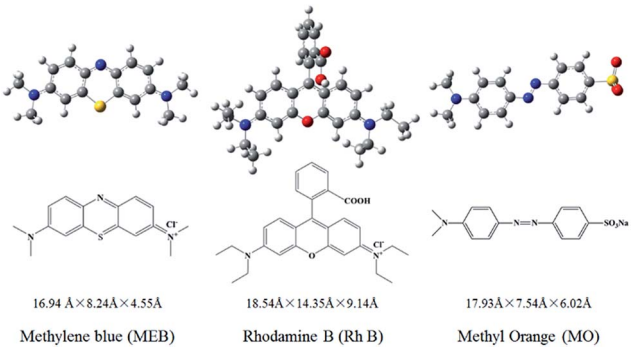

Fig. 6 The structures and dimensions of the dyes MEB, RhB, and MO.

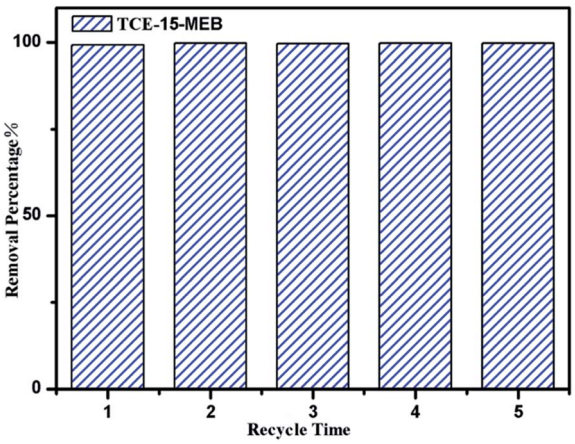

Fig. 8 Reusability of the polymer POP-TCE-15 for removing MEB.

was considered, the adsorption of POP-TCE-15 to the dyes should be in the reverse order of MEB > MO > RhB, which did not match with the experimental results of MEB > RhB ≫ MO.

Therefore, we adopted ESP analysis to further explore the reasons for the adsorption order. The ESP surfaces (isosurface of electron density = 0.001 au) with the most negative surface ESPs ($V_{s,min}$) or the most positive surface ESPs ($V_{s,max}$) are depicted in Fig. S5 (ESI†). The ESP surfaces of dyes MEB and RhB are shown in blue and have a $V_{s,max}$ of 84.60 kcal mol^{-1} and 96.46 kcal mol^{-1}, respectively. In contrast, the ESP of dye MO is negative and is shown in red. The cavity of crown-ether-15 is also shown in red, with a $V_{s,min}$ of −57.36 kcal mol^{-1}, suggesting that it is easy to adsorb cations rather than anions. The ESP analysis confirms that it is favorable for crown-ether-15 to adsorb MEB and RhB but not MO through electrostatic interaction.

Considering the size effect, which coexists with electrostatic interaction, the size of RhB is much larger than MEB, which decreases the trend for it to be absorbed by the probe. Furthermore, the interaction energy has also been calculated through finding the energy difference between the complexes and two molecules. One of the possible adsorption models is shown in Fig. 7. The computed interaction energy gives a result with the order MEB > RhB ≫ MO, which is fully in accordance with the experimental results.

The pH studies and adsorption isotherms suggest that POP-TCE-15 possesses an efficient adsorption properties for MEB due to the hydrophobicity, high surface area, and electrostatic interaction, which indicates that the MEB can be recovered from POP-TCE-15 by rinsing with water/ethanol. The maximum desorption efficiency is 93%. To demonstrate the reusability of the POP-TCE-15 adsorbent, an adsorption–desorption cycle was repeated five times. As Fig. 8 shows, the adsorption capacity of the POP-TCE-15 adsorbent does not significantly change during the adsorption–desorption recycling. The results indicate that the POP-TCE-15 adsorbent is qualified for efficient removal of dyes from aqueous solutions.

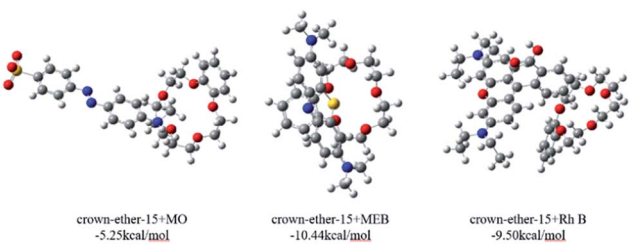

Fig. 7 Optimized structures for the complexes and interaction energy.

Conclusions

The novel triptycene and crown ether-based porous copolymer POP-TCE-15 bearing many attractive features, such as high surface area, good microporosity, hydrophobicity, and high densities of O heteroatom groups, was successfully synthesized by a convenient and efficient Friedel–Crafts reaction. The synthesized POP-TCE-15 adsorbent showed a superior adsorption capacity (up to 787.4 mg g^{-1}) for MEB adsorption, but only one-tenth as much for the anionic dye MO. The high adsorption capacity is due to the electrostatic interaction between the positively charged cationic MEB and the lone pair of electrons on the O atoms of crown-ether-15. However, although POP-TCE-15 adsorbed only one-tenth as much MO, it could more effectively be reused with little loss of adsorption capacity. The convenient and low cost synthesis, coupled with the excellent adsorption properties, make this novel polymer POP-TCE-15 an attractive adsorbent for dye removal.

Conflicts of interest

There are no conflicts of interest to declare.

Acknowledgements

This work is supported by the National Key Basic Research Program of China (2015CB251401) and the Natural Science Foundation of China (No. 21476070, 21776069).

References

1 D. Pokhrel and T. Viraraghavan, *Sci. Total Environ.*, 2004, **333**, 37–58.

2 C. O'Neill, F. R. Hawkes, D. L. Hawkes, N. D. Lourenço, H. M. Pinheiro and W. Delée, *J. Chem. Technol. Biotechnol.*, 1999, **74**, 1009–1018.
3 X. D. Du, C. C. Wang, J. G. Liu, X. D. Zhao, J. Zhong, Y. X. Li, J. Li and P. Wang, *J. Colloid Interface Sci.*, 2017, **506**, 437–441.
4 E. Alver and A. Ü. Metin, *Chem. Eng. J.*, 2012, **200–202**, 59–67.
5 A. Walcarius and L. Mercier, *J. Mater. Chem.*, 2010, **20**, 4478–4511.
6 D. Mohan, K. P. Singh and V. K. Singh, *J. Hazard. Mater.*, 2008, **152**, 1045–1053.
7 I. Ali, *Chem. Rev.*, 2012, **112**, 5073–5091.
8 T. K. Mahto, S. Chandra, C. Haldar and S. K. Sahu, *RSC Adv.*, 2015, **5**, 47909–47919.
9 A. B. Dichiara, T. J. Sherwood, J. Benton-Smith, J. C. Wilson, S. J. Weinstein and R. E. Rogers, *Nanoscale*, 2014, **6**, 6322.
10 W. Lei, D. Portehault, D. Liu, S. Qin and Y. Chen, *Nat. Commun.*, 2013, **4**, 1777.
11 H. P. Cong, X. C. Ren, P. Wang and S. H. Yu, *ACS Nano*, 2012, **6**, 2693–2703.
12 S. Lu, Y. Hu and W. Zhang, *J. Am. Chem. Soc.*, 2017, **139**, 17082–17088.
13 L. Li, H. Zhao, J. Wang and R. Wang, *ACS Nano*, 2014, **5**, 5352–5364.
14 Y. Du, H. Yang, J. M. Whiteley, S. Wan, Y. Jin, S. H. Lee and W. Zhang, *Angew. Chem., Int. Ed.*, 2016, **55**, 1737–1741.
15 Y. Wu, M. Zhang, H. Zhao, S. Yang and A. Arkin, *RSC Adv.*, 2014, **4**, 61256–61267.
16 H. J. Zhang, J. H. Wang, Y. H. Zhang and T. L. Hu, *J. Polym. Sci., Part A: Polym. Chem.*, 2017, **55**, 1329–1337.
17 Y. He, T. Xu, J. Hu, C. Peng, Q. Yang, H. Wang and H. Liu, *RSC Adv.*, 2017, **7**, 30500–30505.
18 C. Yan and B. Han, *J. Am. Chem. Soc.*, 2012, **134**, 6084–6087.
19 Y. He, X. Zhu, Y. Li, C. Peng, J. Hu and H. Liu, *Microporous Mesoporous Mater.*, 2015, **214**, 181–187.
20 W. Song, X. Xu, Q. Chen, Z. Zhuang and X. Bu, *Polym. Chem.*, 2013, **4**, 4690.
21 L. Chen, K. Furukawa, J. Gao, A. Nagai, T. Nakamura, Y. Dong and D. Jiang, *ChemComm*, 2014, **136**, 9806–9809.
22 S. Wan, J. Guo, J. Kim, H. Ihee and D. Jiang, *Angew. Chem., Int. Ed.*, 2009, **48**, 5439–5442.
23 E. Haque, V. Lo, A. I. Minett, A. T. Harris and T. L. Church, *J. Mater. Chem. A*, 2014, **2**, 193.
24 A. D. Becke, *Phys. Rev. A*, 1988, **38**, 3098–3100.
25 C. Lee, W. Yang and R. G. Parr, *Phys. Rev. B*, 1988, **37**, 785–789.
26 J. A. Pople, M. Head-Gordon and K. Raghavachari, *J. Chem. Phys.*, 1987, **87**, 5968.
27 M. J. Frisch, G. W. Trucks, H. B. Schlegel, G. E. Scuseria, M. A. Robb, J. R. Cheeseman, G. Scalmani, V. Barone, B. Mennucci, G. A. Petersson, H. Nakatsuji, M. Caricato, X. Li, H. P. Hratchian, A. F. Izmaylov, J. Bloino, G. Zheng, J. L. Sonnenberg, M. Hada, M. Ehara, K. Toyota, R. Fukuda, J. Hasegawa, M. Ishida, T. Nakajima, Y. Honda, O. Kitao, H. Nakai, T. Vreven, J. A. Montgomery Jr, J. E. Peralta, F. Ogliaro, M. Bearpark, J. J. Heyd, E. Brothers, K. N. Kudin, V. N. Staroverov, R. Kobayashi, J. Normand, K. Raghavachari, A. Rendell, J. C. Burant, S. S. Iyengar, J. Tomasi, M. Cossi, N. Rega, J. M. Millam, M. Klene, J. E. Knox, J. B. Cross, V. Bakken, C. Adamo, J. Jaramillo, R. Gomperts, R. E. Stratmann, O. Yazyev, A. J. Austin, R. Cammi, C. Pomelli, J. W. Ochterski, R. L. Martin, K. Morokuma, V. G. Zakrzewski, G. A. Voth, P. Salvador, J. J. Dannenberg, S. Dapprich, A. D. Daniels, O. Farkas, J. B. Foresman, J. V. Ortiz, J. Cioslowski and D. J. Fox, *Gaussian 09, Revision A*, Gaussian, Inc., Wallingford CT, 2009.
28 T. Lu and F. Chen, *J. Comput. Chem.*, 2012, **33**, 580–592.
29 B. Li, R. Gong, W. Wang, X. Huang, W. Zhang, H. Li, C. Hu and B. Tan, *Macromolecules*, 2011, **44**, 2410–2414.
30 J. Weber and A. Thomas, *J. Am. Chem. Soc.*, 2008, **1**, 2–3.
31 L. Meng, X. Zhang, Y. Tang, K. Su and J. Kong, *Sci. Rep.*, 2015, **5**, 7910.
32 K. Zarrini, A. A. Rahimi, F. Alihosseini and H. Fashandi, *J. Cleaner Prod.*, 2017, **142**, 3645–3654.
33 W. Stawiński, A. Węgrzyn, O. Freitas, L. Chmielarz and S. Figueiredo, *Microporous Mesoporous Mater.*, 2017, **250**, 72–87.
34 V. C. Srivastava, M. M. Swamy, I. D. Mall, B. Prasad and I. M. Mishra, *Colloids Surf., A*, 2006, **272**, 89–104.
35 J. Chang, J. Ma, Q. Ma, D. Zhang, N. Qiao, M. Hu and H. Ma, *Appl. Clay Sci.*, 2016, **119**, 132–140.
36 Y. Li, Q. Du, T. Liu, X. Peng, J. Wang, J. Sun, Y. Wang, S. Wu, Z. Wang, Y. Xia and L. Xia, *Chem. Eng. Res. Des.*, 2013, **91**, 361–368.
37 J. Fu, Z. Chen, M. Wang, S. Liu, J. Zhang, J. Zhang, R. Han and Q. Xu, *Chem. Eng. J.*, 2015, **259**, 53–61.
38 C. Zhang, P.-C. Zhu and B. Tian, *Macromolecules*, 2015, **48**, 8509–8514.
39 X. Zhu, S. An and Y. Liu, *AIChE J.*, 2017, **63**, 3470–3478.